CHAPTER IV

DEVELOPMENT OF THE TRACTION MODEL FOR THE PROTOTYPE TRACK

4.1. INTRODUCTION

Based on the literature review in Chapter 2, analytical methods of modeling were preferred to other method for this research. For analytical methods fewer parameters were needed to be measured with than methods such as the finite element analysis (FEM). Analytical methods also offered closer simulation to the real tractive phenomenon than the empirical approaches such as the methods based on cone index.

After years of research and assessment by researchers, analytical methods for soil characterization and traction modelling based on the bevameter technique is still a preferred technique. For its feasibility and simplicity, the approach based on bevameter technique was therefore chosen for this research.

To develop the traction model by applying analytical methods based on the bevameter technique, characteristics of the friction between the track and the terrain surface, limited soil shear characteristics, and the pressure-sinkage relationship had to be determined. The soil parameters and the distribution of the contact pressure could be applied for the prediction of the tractive performance. By applying Bekker's analysis of motion resistance, mainly caused by soil compaction and the loss from internal track friction, the total motion resistance could be predicted.

The distribution of the contact and tangential stresses relies mainly on the deformation of the track and the terrain surface. When the bevameter technique was applied to predict the distribution and magnitude of the ground contact pressure under the track, the shape of the deflected track in contact with the terrain surface

was of importance. A detailed analysis of the pressure distribution at the track–terrain interface was made. For traction modelling the relationship between the relevant vehicle parameters associated with the deformed track shape in contact with the terrain and the soil characteristics was established.

4.2 CHARACTERIZATION OF RUBBER-SOIL FRICTION AND SOIL SHEAR WITH DISPLACEMENT

As reviewed and discussed in the preceding chapters, the thrust between the running gear and the terrain surface, for a traditional tractive device, is usually developed by the internal soil shearing action associated with relative slip. It is the rationale that the prototype track generates tractive thrust mainly by friction between the smooth rubber surface and the terrain surface whilst the soil-soil shear is minimal. The characterization of the relationship for soil shear stress versus shear displacement, and soil-rubber friction versus displacement was thus required for the proposed modelling procedure.

When the shear action occurs in the soil, which is typical for a tractive device with grousers moving over a soft terrain surface, the maximum shear stress τ_{max} can be described by the Mohr-Coulomb failure equation, i.e. equation 2.11.

The Mohr-Coulomb equation describes the shear strength of soil to soil, therefore it is valid when used to simulate the shearing action of a tyre or track with lugs penetrating into the soil. Shear action in the soil is caused by the moving lugs when the running gear propels the vehicle. However, when the surface of the running gear is smooth and the slip action apparently occurs at the soil contact surface, it is more appropriate to describe the phenomenon as frictional. Thus it is better expressed by applying another equation of similar form but with different parameters for the maximum frictional stress τ_{fmax} at the frictional contact surface as expressed by:

$$\tau_{fmax} = c_a + p \tan \delta \tag{4.1}$$

where

c_a = soil-rubber adhesion on the interacting surface, (Pa).

p = contact stress on the interacting surface, (Pa).

δ = angle of soil-rubber friction, (degrees).

From the preparatory field measurements in this research, the values of the soil shear parameters obtained from steel shear grousers were different from the measured friction-shear parameters obtained by using the rubber-coated track element as a friction plate with a smooth rubber surface (Yu, 1996). It was also found that the values of the coefficient of soil to rubber surface friction tan δ, and the internal shearing resistance of the soil tan φ were very similar as shown in Table 4.1. The adhesion between rubber and soil was less than the internal cohesion of the soil. This was in accordance with values reported by Neal (1966) and Wills (1963). Therefore the two cases of soil shear and rubber-soil friction must be considered differently for traction modelling.

Table 4.1. Comparison of soil internal shear and soil-rubber friction parameters (Yu, 1996).

Soil water content (dry basis), %	Internal frictional angle for soil shear ϕ, degrees	Soil internal cohesion c, kPa	Soil-rubber frictional angle δ, degrees	Soil-rubber adhesion c_a, kPa
10.9	33.9	1.62	29.4	1.55
21.6	31.1	2.59	29.9	2.69
35.3	30.9	3.34	28.7	2.49

The tractive thrust for the prototype track under investigation is generated by the smooth rubber surface when the track, composed of individual track elements, develops pull on soft terrain surface. For the interaction between the track element and the soil surface, the soil-rubber frictional action is dominant, rather than the

internal soil shear action applicable for conventional steel tracks with grousers. The rubber-soil friction characterization can adequately represent the interaction between the prototype track and soil surface.

According to the measured data for the rubber track element collected during the *in situ* tests, the tangential frictional stress initially increased rapidly with the increase in displacement, and then approaches an approximately constant value for a further increase in displacement as shown in Figure 4.1 (Yu & du Plessis, 1997).

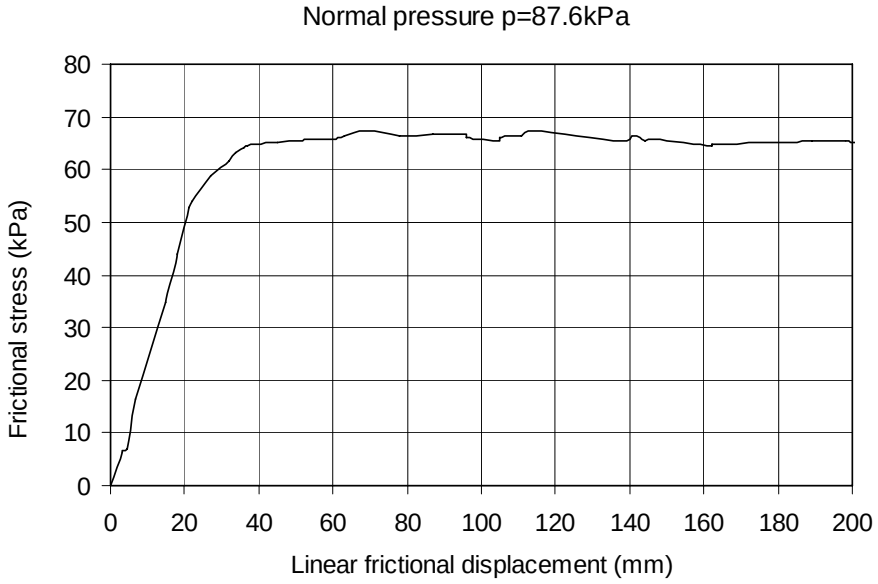

Figure 4.1. Frictional stress versus displacement for a track element test.

Such type of relationship between the shear-friction stress and the displacement as shown in Figure 4.1 can be expressed as equation (2.6) (page 2-11) by an exponential equation similar to the one proposed by Janosi and Hanamoto (1961). This equation can be modified to express the relationship of rubber-soil friction versus corresponding displacement as follow:

$$\begin{aligned} \tau_f &= \tau_{f\,max}\,(1 - e^{-j/K}) \\ &= (c_a + p\tan\delta)(1 - e^{-j/K}) \end{aligned} \tag{4.2}$$

where

τ_f = rubber-soil frictional stress, (Pa).

j = relative tangential displacement for soil-rubber friction, (m).

K = frictional deformation modulus, (m).

Equation (4.2) reflects the relationship between the horizontal contact frictional stress and the corresponding slip below the prototype track and soil and is thus used as the basic soil-rubber frictional characterization.

When compared to the Janosi-Hanamoto equation (2.6), equation (4.2) has the same format for the equation and also the number of parameters. However, the terms of the parameters in the equation have different physical meanings. It is the fundamental relationship for calculating the total tractive effort in the horizontal direction in this research.

To obtain the parameters related to the frictional characteristics from the field tests, the method based on the bevameter technique and the procedure reported by Wong (1989, 1993) and Upadayaya (1994) was adapted.

4.3 CHARACTERIZATION OF THE RELATIONSHIP BETWEEN CONTACT PRESSURE AND SINKAGE

The maximum shear or frictional stress between the tractive device and the terrain surface directly depends on the applied contact pressure. On a soft terrain surface the contact pressure is usually related to the sinkage. As reviewed in Chapter 2, several efforts have been made to identify the exact relationship for contact pressure versus sinkage in both agricultural engineering and civil engineering applications. To describe the relationship of the contact pressure and the corresponding sinkage, the expression proposed by Bekker is still the most common one applied for analytical modelling methods to predict vehicle performance, especially for the case of soft terrain surfaces.

The relationship of contact pressure and sinkage expressed by equation (2.1) can be used to calculate the contact pressure at each point on the ground contact surface under the track. In equation (2.1), k_c and k_ϕ are parameters related to steel-soil cohesion and soil-soil friction respectively, while n is the exponent for sinkage deformation.

For the experimental work, the parameters obtained and the resulted curves from the field tests are presented in the results.

4.4 ANALYSIS OF THE DISTRIBUTION OF TRACK-SOIL CONTACT PRESSURE

The analysis by Wills (1963) proved that the contact pressure distribution influences the development of tractive effort. The prediction of the distribution of the contact pressure is therefore one of the most important issues in analytical traction modelling for wheels and tracks.

To a large extent, the shape of the track in contact with the terrain surface governs the distribution of contact pressure. Several typical track deformation shapes can be considered.

4.4.1 Tractive effort for uniform and trapezoidal pressure distribution

The initial design of the prototype track tested in this project was aimed to achieve an ideally almost uniform contact pressure distribution by applying the walking beam concept. For most of the conventional steel tracks, however, the pressure distribution for a uniformly loaded track was far from being uniform, as reported by many researchers (Wills, 1963; Wong, 1989). For the practical situations, several factors influence the pressure distribution at the contact surface including vehicle and track physical parameters, soil homogeneity and other soil physical properties and in particular the weight transfer of the tractor. To counterbalance the effect of weight

transfer, some means of automatic adjustment of the vertical load and consequently the centre of gravity must be utilized, which is not yet realized for practical field operations.

When any drawbar pull is applied, the intensity and the distribution of the ground contact pressure below the track is influenced by weight transfer. To take into account the effect of the weight transfer, the position of the centre of gravity (CG) of the test tractor was designed to be located in front of the centre of the track contact length. When a drawbar pull is applied, the load distribution center of the ground contact pressure for the track moves rearwards, caused by weight transfer.

In this research project, two simple models of contact pressure distribution are initially validated and analyzed. One is a uniform distribution whilst the other a dynamic trapezoidal distribution (Figure 4.2). In the dynamic trapezoidal model, to predict the distribution of the vertical load, the effect of the weight transfer caused by drawbar pull is taken into consideration.

For the uniform distribution of the contact pressure, as shown in Figure 4.2 (b), the value of the ground contact pressure p (Pa) can be calculated from:

$$p = W / A \tag{4.3}$$

where

W = the total vertical load on one track including track weight, (N).

A = the total contact area of one track, (m^2).

For the trapezoidal contact pressure distribution, as shown in Figure 4.2 (a) and (c), the contact pressure changes when the drawbar pull increases. For the static state and without drawbar pull, the centre of gravity for the vehicle is located in front of the centre point of the track, thus the contact pressure has a larger magnitude at the front end and decreases rearwards. As the drawbar pull increases to a specified value, the transient state of ideal uniform distribution for the contact pressure below the track

may be reached as shown in Figure 4.2 (b). When the drawbar pull increases further, the magnitude of the contact pressure at the front end of the track decreases and is smaller than at the rear (Figure 4.2 (c)).

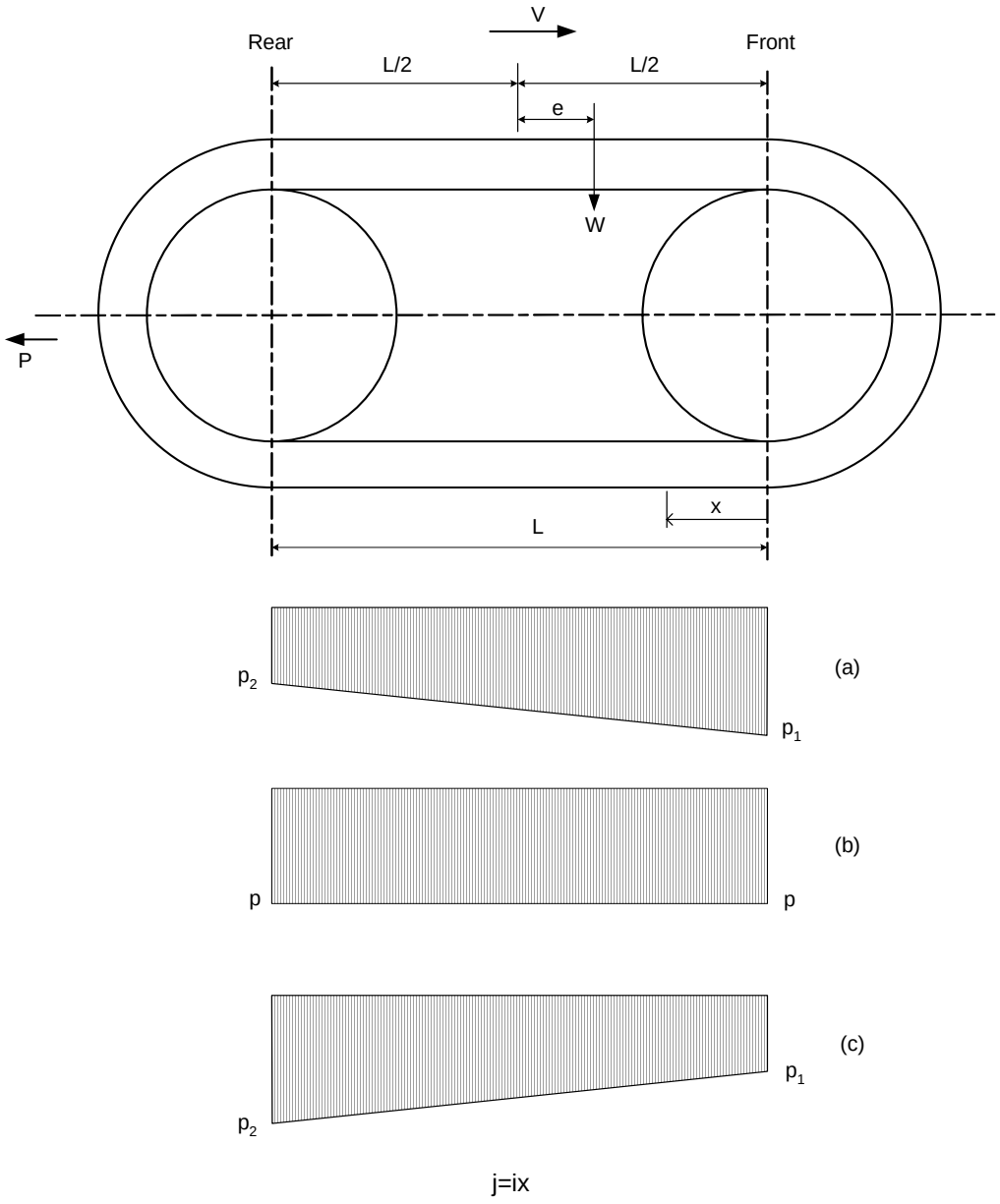

Figure 4.2. The idealized distribution of contact pressure under a track.

In both cases of distribution (a) and (c), if it is assumed that the tractor does not tilt, one obtains:

$$p = \frac{p_1 + p_2}{2} = \frac{W}{A} = \frac{W}{bL} \tag{4.4}$$

Where b is the width (m) and L (m) the contact length of one track.

In Figure 4.2 (a), the contact pressure p(x) for any point at a distance x from the track front contact point can be calculated from:

$$p(x) = p_2 + (p_1 - p_2)\frac{L - x}{L} \tag{4.5}$$

where p(x) is the contact pressure at a distance x from the track front contact point.

Similarly, in Figure 4.2 (c), p(x) can be calculated from:

$$p(x) = p_1 + (p_2 - p_1)\frac{x}{L} \tag{4.6}$$

For either a uniform or trapezoidal contact pressure, it is assumed that the friction-shear displacement j is linearly proportional to the track slip i. At any point below the track, with distance x to the front end of the track, the value of the friction-shear displacement between track and soil, as shown in Figure 4.2, is given by:

$$j = ix \tag{4. 7}$$

where i is the slip of the track.

Substituting equation (4.7) into equation (4.2),

$$\begin{aligned} \tau_f &= \tau_{f\,max}(1 - e^{-j/K}) \\ &= (c_a + p\tan\delta)(1 - e^{-ix/K}) \end{aligned} \tag{4. 8}$$

where the contact pressure p is also a function of x and is expressed by one of equations (4.3) to (4.6).

When the frictional stress τ_f is integrated along the contact length, the total tractive effort F_t can be predicted as:

$$F_t = 2\int_0^L \tau_f(x)dx$$
$$= 2\int_0^L [c_a + p(x)\tan\delta](1 - e^{-ix/K})dx \quad (4.9)$$

4.4.2 Tractive effort for a rigid track model with tilt angle

On a deformable terrain surface, however, the track-soil contact surface is usually inclined towards the rear of the track, depending on the drawbar height and drawbar pull. With further assumption of a tilt angle β, the parameters to describe the track-soil interaction are illustrated in Figure 4.3.

As shown in Figure 4.3, for equilibrium in the vertical direction:

$$W = b\int_0^L [p(x)\cos\beta + \tau_f(x)\sin\beta]dx \quad (4.10)$$

For equilibrium in the horizontal direction:

$$F_t = b\int_0^L [\tau_f(x)\cos\beta - p(x)\sin\beta]dx \quad (4.11)$$

and the rolling resistance R_r:

$$R_r = b\int_0^L p(x)\sin\beta dx \quad (4.12)$$

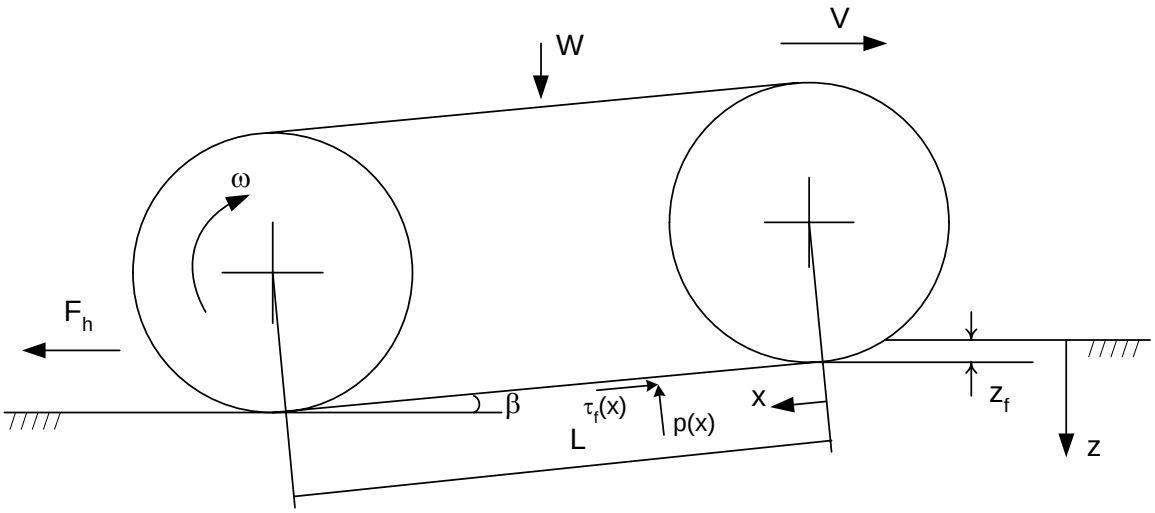

Figure 4.3. Side view of the track-soil interaction with the inclusion of a tilt angle.

In the above equations (4.10-4.12), the contact pressure of the track at any point in contact with the terrain depends on the corresponding sinkage at the specific point, whilst the sinkage can be calculated from the initial sinkage of the front wheel z_{f0} and the tilt angle β.

By substituting the values of $\tau_f(x)$ and $p(x)$ into the above equations, the tractive effort F_t and the rolling resistance R_r can be predicted.

The calculation for traction can be initiated by assuming that the front and rear wheels support the total static vertical load proportionally. The static sinkage of the front and the rear wheels can be calculated by applying the equation proposed by Bekker (1960). The tilt angle can also be calculated according to the load distributed on the front and rear wheels respectively.

To avoid a negative tilt angle, the tilt angle is initially assumed to be zero, due to the fact that the CG of the tractor is located in front of the middle point of the track in a longitudinal direction. The tilt angle remains zero until the vertical load is distributed equally between the front and the rear wheels. With further increase in drawbar pull, the load on the rear wheels increases and the load on the front wheels decreases by the same numeric value which was derived from the weight transfer. The tilt angle is

taken into consideration as soon as the load on the rear wheels is larger than the load on the front wheels.

Therefore, one of the advantages of this model is that the effect of load transfer can be accounted for when the drawbar pull changes, in addition to the uniform or trapezoidal contact pressure distributions.

4.4.3 Tractive effort for the flexible track model

If the designed walking beam effect of the prototype track materializes, the track operates similar to a wheel of very large diameter which may result in a very uniform distribution of contact pressure. The track-soil interaction can be solved by applying one of the idealized models as shown in Figures 4.2 and 4.3.

However, when the centre wheels were not forced onto the track, it was difficult to achieve the idealized uniformly distributed contact pressure as envisaged by the original design concept. Most likely, the track was flexible and be deformed at the section between the front and the rear wheels, being influenced by several factors, particularly the terrain characteristics and the track tension. When the track tension was not automatically adjusted or not sufficient to form the large circle in equilibrium with the terrain, the section of the track between the front and rear wheels would be deflected upwards and form a curved interacting shape with the terrain surface. The shape of this interaction surface would, to a large extent, govern the distribution of the contact pressure.

While the ideal contact pressure distribution is as shown in Figure 4.2, based on the practical observations and preparatory tests on a soft terrain surface (Yu and du Plessis, 1997) definitive peak pressures were observed below the front and rear wheels. The shape of the flexible interaction surface between the track and the soil was assumed to be as shown in Figure 4.4.

For the shape shown in Figure 4.4, the contact surface of the track and deformable terrain can be divided into two typical segments, one in contact with both the wheel and terrain, such as segments of ABC and FGH, and another in contact only with the terrain, such as segment CDEF.

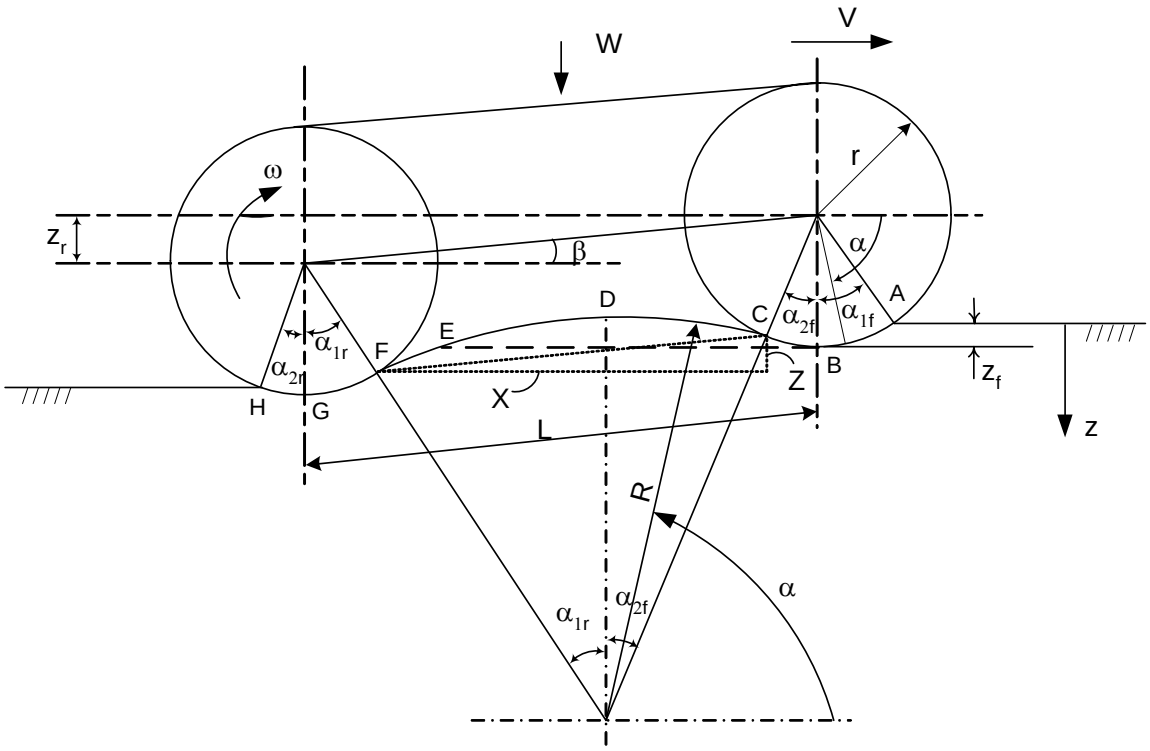

Figure 4.4. The flexible deformation model for track-soil interaction.

It was assumed that the front wheels initially had a sinkage of z_f, and the shape of the curve between the front and the rear wheels, i.e. the segment CDEF in contact only with the terrain surface, was circular in shape, with radius R.

On a soft terrain surface, the inflation pressure of the driving and tension wheels was relatively high to optimize the friction drive. It is, therefore, reasonable to assume that the wheels have characteristics similar to that of rigid wheels. The shape of the contact segments ABC and FGH therefore are circular, with the same diameter as the tyres.

On the basis of the assumptions above, the following relevant geometrical parameters were derived from the track-soil configuration as illustrated in Figure 4.4.

$$\alpha_{1f} = \cos^{-1}(1 - \frac{z_f}{r}) \tag{4.13}$$

$$R = \frac{\sqrt{X^2 + Z^2}}{2\sin[(\alpha_{1r} + \alpha_{2f})/2]} \tag{4.14}$$

where

$$X = L\cos\beta - r(\sin\alpha_{1r} + \sin\alpha_{2f}) \tag{4.15}$$

and

$$Z = L\sin\beta - r(\cos\alpha_{1r} - \cos\alpha_{2f}) \tag{4.16}$$

$$\beta = \sin^{-1}((z_r - z_f)/L) \tag{4.17}$$

$$\alpha_{1r} = \alpha_{2f} + 2\beta \tag{4.18}$$

If a rigid wheel on a soft terrain was accepted, the sinkage of the front and the rear wheels could be determined by applying the analysis as proposed by Bekker (1956, 1960):

The sinkage

$$z_f = \left[\frac{3W_f}{b(3-n)(k_c/b + k_\phi)\sqrt{2r}}\right]^{2/(2n+1)} \tag{4.19}$$

and sinkage

$$z_r = \left[\frac{3W_r}{b(3-n)(k_c/b + k_\phi)\sqrt{2r}}\right]^{2/(2n+1)} \tag{4.20}$$

where W_f and W_r represented the vertical load on the front and the rear wheels respectively whilst b was the track width

In the above analysis, the radius of the deformed track segment in contact with the terrain surface directly depended on the exit angle of the front wheels, the distance between the front and the rear wheels and the wheel diameter.

Wong (1989) indicated that the entrance and the exit angles for a pneumatic tyre were interrelated and the relationship was governed by the terrain response to repetitive contact loading, but the relationship was not specified or suggested. Due to the fact that the rebound of the terrain was limited by the track tension and the track was not definitely flexible, the exit angle was expected to be smaller than the value calculated for the case of a pneumatic tyre.

Okello et al (1998) proposed the use of a constant C to relate the entrance and the exit angles as:

$$\alpha_{2r} = C\alpha_{1f} \tag{4.21}$$

However, no method to determine the value of C was mentioned.

From the curves of the repetitive contact loading, it could be seen that when the terrain stiffness was larger, the contact pressure decreased more rapidly during the unloading cycle and the elastic rebound of the terrain took a shorter period of time. It was considered that the slope angle of the unloading curve could be used to derive the exit angle. No practical conclusions on the entrance and exit angles were drawn from the unloading-reloading curves and it needs more experimentation to proof such a relationship.

Karafiath and Nowatzki (1978, pp 386-387) proposed that the exit angle be taken as 10 degrees for entry angle variations from 30 to 60 degrees. For entry angles of less than 30 degrees, it should be reduced by half the difference between the entry angle

and 30 degrees. Based on this method, the exit angle was therefore calculated as 0 when the entry angle was less than 10 degrees. By considering the effect of the track tension on soft terrain for the proposed model, the exit angle was determined as one third of the entry angle.

The track contact surface was divided into n segments of different configuration, and the equilibrium equations for the track were expressed as:

In the vertical direction,

$$\begin{aligned} W &= \sum_{i=1}^{n} W_i \\ &= \sum_{i=1}^{n} b\int_0^{l_i} (p_i \sin\alpha + \tau_{fi}\cos\alpha)dx \\ &= \sum_{i=1}^{n} b\int_{\alpha_i}^{\alpha_{i+1}} r_i(p_i \sin\alpha + \tau_{fi}\cos\alpha)d\alpha \end{aligned} \tag{4.22}$$

In the horizontal direction,

$$\begin{aligned} F_t &= \sum_{i=1}^{n} F_{ti} \\ &= \sum_{i=1}^{n} b\int_0^{l_i} (p_i \cos\alpha + \tau_{fi}\sin\alpha)dx \\ &= \sum_{i=1}^{n} b\int_{\alpha_i}^{\alpha_{i+1}} r_i(p_i \cos\alpha + \tau_{fi}\sin\alpha)d\alpha \end{aligned} \tag{4.23}$$

In the above equations, the subscription i indicates the i^{th} segment which has the length of ℓ_i with radius of r_i, entrance angle of α_i and exit angle of α_{i+1} under consideration, as illustrated in Figure 4.4. It can be seen that all the variables in the above equations can be expressed as functions of the angle α of the wheels.

To describe the relationship of the frictional-shear stress versus the slippage (j), an analysis based on Wong's model for a steel track with ground wheels (Wong, 1993), was adopted.

The slip velocity of any point on the surface of the track-soil interaction, relative to the terrain surface, was the tangential component of the absolute velocity:

$$\begin{aligned} V_j &= V_t - V\sin\alpha \\ &= r\omega - r\omega(1-i)\sin\alpha \\ &= r\omega[1-(1-i)\sin\alpha] \end{aligned} \tag{4.24}$$

The friction-shear displacement (j) along the track-terrain interface was obtained by integrating the slip velocity from the point where friction-shear started to the specified point under consideration:

$$\begin{aligned} j &= \int_0^t r\omega[1-(1-i)\sin\alpha]dt \\ &= \int_{\pi/2-\alpha_{1f}}^{\alpha_i} r[1-(1-i)\sin\alpha]d\alpha \\ &= \ell - (1-i)x \end{aligned} \tag{4.25}$$

where ℓ is the contact length between the specified point to the point where soil contact started, and x was the corresponding horizontal distance between the specific point and the initial soil contact point. The rotational angle α for each segment was considered. The value of α_i was calculated according to the corresponding configuration of the segment. Therefore the integrated value of j was also calculated for any point within each segment. For instance, for the segment ABC, the friction and shear displacement j at any point was calculated as:

$$\begin{aligned} j &= r[(\alpha-(\pi/2-\alpha_{1f}))+(1-i)(\cos\alpha-\cos(\pi/2-\alpha_{1f}))] \\ &= r[(\alpha-(\pi/2-\alpha_{1f}))+(1-i)(\cos\alpha-\sin\alpha_{1f})] \end{aligned} \tag{4.26}$$

Whilst for a point within the segment of the track in contact only with the terrain surface CDEF, j was calculated from:

$$\begin{aligned} j &= \int_{\pi/2-\alpha_{1f}}^{\pi/2+\alpha_{2f}} r[1-(1-i)\sin\alpha]d\alpha + \int_{\pi/2-\alpha_{2f}}^{\alpha} r[1-(1-i)\sin\alpha d\alpha \\ &= r[(\alpha_{1f}+\alpha_{2f})-(1-i)(\sin\alpha_{1f}+\sin\alpha_{2f})] \\ &\quad + r[(\alpha-(\pi/2-\alpha_{2f}))+(1-i)(\cos\alpha-\sin\alpha_{2f})] \end{aligned} \tag{4.27}$$

Similarly, for a point within the segment FGH, the displacement was determined from:

$$\begin{aligned} j &= \int_{\pi/2-\alpha_{1f}}^{\pi/2+\alpha_{2f}} r[1-(1-i)\sin\alpha]d\alpha + \int_{\pi/2-\alpha_{2f}}^{\pi/2+\alpha_{1r}} R[1-(1-i)\sin\alpha d\alpha \\ &\quad + \int_{\pi/2-\alpha_{1r}}^{\alpha} r[1-(1-i)\sin\alpha]d\alpha \\ &= r[(\alpha_{1f}+\alpha_{2f})-(1-i)(\sin\alpha_{1f}+\sin\alpha_{2f})] \\ &\quad + R[(\alpha_{2f}+\alpha_{1r})-(1-i)(\sin\alpha_{2f}+\sin\alpha_{1r})] \\ &\quad + r[(\alpha-(\pi/2-\alpha_{1r}))+(1-i)(\cos\alpha-\sin\alpha_{1r})] \end{aligned} \tag{4.28}$$

4.5 THE PREDICTION OF MOTION RESISTANCE

The motion resistance of the prototype track R_r can be expressed as:

$$R_r = R_e + R_i \tag{4.29}$$

Where R_e is the external resistance and R_i is the internal track resistance.

For the models as discussed in the Section 4.4.1 (page 4-5), the external motion resistance between the track and the terrain surface is mainly due to the soil compaction below the track. To simplify the procedure for predicting the performance, only the rolling resistance for soil compacting was taken into consideration.

If the contact pressure on the track-terrain interface is distributed uniformly, which is the case for an ideal ground pressure distribution based on the initial design, the motion resistance for compacting soil was expressed by Bekker (1960):

$$R_e = \frac{b}{(n+1)(k_c/b+k_\phi)^{(1/n)}}\left(\frac{W}{bL}\right)^{(n+1)/n} \tag{4.30}$$

Observations based on the preliminary test results (Yu and du Plessis, 1997) proved that the contact pressure distribution was not as uniform as expected. Other possible pressure distributions, such as the rigid and the flexible track models described in the preceding sections, should therefore also be considered. For both rigid and flexible models, the rolling resistance was attributed to the total horizontal component of the contact pressure in the direction opposite to travelling. The contact pressure was expressed as a function of the rotational angle of the track segment α for the flexible track model as shown in Figure 4.4. The motion resistance can be predicted by summation of the motion resistance generated by each segment of the track as shown in the following equation:

$$\begin{aligned} R_e &= \sum_{i=1}^{n} R_i \\ &= \sum_{i=1}^{n} b \int_0^{\ell_i} p(x) \sin \alpha \, d\ell \\ &= \sum_{i=1}^{n} b r_i \int_{\alpha_i}^{\alpha_{i+1}} p(x) \sin \alpha \, d\alpha \end{aligned} \tag{4.31}$$

In Equation (4.31), ℓ_i is the corresponding length of the i^{th} track segment, whilst r_i is either the radius of the wheels or the virtual radius of the circular curve of the track in contact only with the terrain surface.

The internal loss is mainly caused by friction and relative movement and associated friction between the track elements. The track tension of the prototype traction system was designed to be adjustable. If the track tension was adjusted to be higher than the maximum tractive effort between the track and terrain surface, the slip resulting would be kept to a minimum.

Under operational conditions, rubber materials have elastic characteristics. During this action extra internal losses were therefore caused by cyclic reshaping of the rubber tracks and the wheels with hysteresis and heat build up. An analysis of the internal resistance will be addressed in the next section.

The total motion resistance can be calculated based on equation (4.29) after the external and internal resistances are obtained.

4.6 INTERNAL TRACK RESISTANCE AND THE FRICTION DRIVE BETWEEN THE WHEEL AND THE TRACK

The prototype track is tensioned to a specified level by a hydraulic cylinder and locked by a threaded rod and lock nuts.

The track tension is a critical factor for the frictional torque transfer between the drive wheels and the internal track surface.

If the rubber surfaced track stretched by the drive wheels is considered as a rubber belt and a rubber pulley, the analytical results for belt conveyers and friction drives may be utilized to explain the relationship of tension and frictional drive force. When the rubber belt track travels on a smooth rigid surface and the traction force is assumed to increase linearly along the ground contact length of the track, as shown in Figure 4.5, the following relationship can be established according to basic theory of belt friction (Green, 1955):

$$\begin{aligned} F_t &= T_t - T_0 \\ &= T_0 e^{\pi' \mu_\varphi} - T_0 \\ &= T_0 e^{(\pi' \mu_\varphi - 1)} \end{aligned} \tag{4.32}$$

where

T_0 = track pre-tension, (N).

T_t = maximum track tention, (N).

F_t = tractive effort, (N).

μ_φ = friction coefficient between contact surfaces.

π' = wrap angle = 180°.

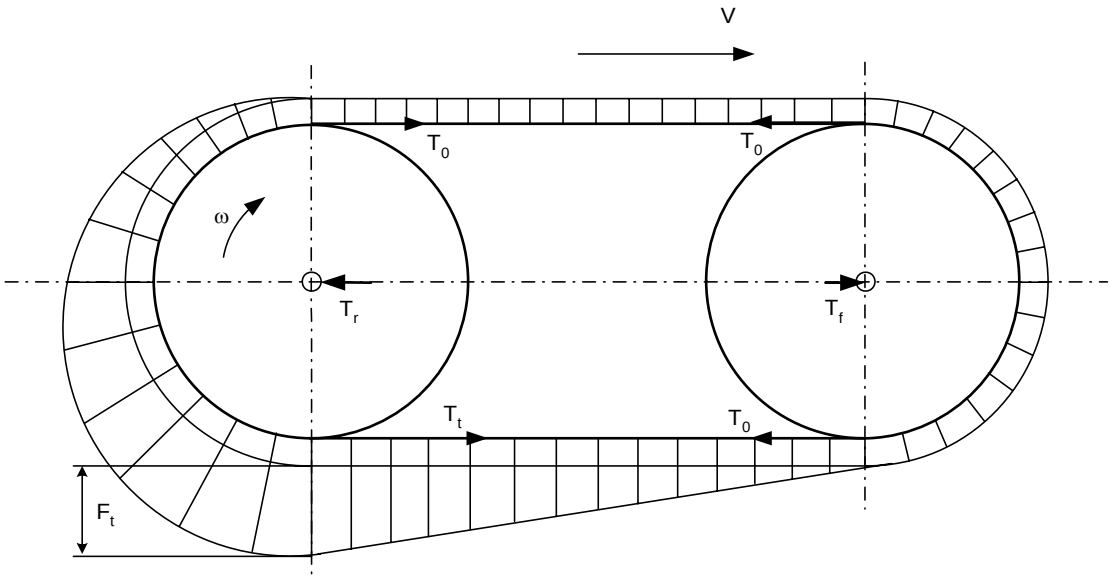

Figure 4.5. Simplified distribution of the track internal tension during forward movement.

When the values of the track pre-tension T_0, the wrap angle and the friction coefficient are set, the tractive effort F_t is the limitation within which slippage is minimized. Therefore the higher the track tension, the larger the traction that can be transfered. On the other hand, the magnitude of the track tension is limited by the dimensions of the sub-frame structure, the strength of the track and other design factors.

As observed in practice, small amounts of slippage occur as soon as the friction drive is loaded, although it is not easily measurable when the drawbar pull is small. The loss caused by this slippage may be accepted as 3-5% of the total power transmitted by the traction device which represents a typical situation for a rubber belt conveyer (Green, 1955).

In this research, to simplify the calculation for modelling, a decrease of 3% of the total tractive effort was accepted to account for internal bending and slip losses, regardless of the speed.

4.7 TOTAL DRAWBAR PULL OF THE PROTOTYPE TRACK

The total drawbar pull F_h is the difference between the tractive effort and the motion resistance and can be expressed as:

$$F_h = F_t - R_r \tag{4.33}$$

where F_t is the resultant total force in the direction of movement which can be obtained by integration or derived from the analysis of tangential stresses and contact pressure. R_r is the total motion resistance.

Since the contact pressure and the tangential stress are functions of the track sinkage and the track slip respectively, the track motion resistance R_r and the tractive effort F_t also vary with the track slip. Based on equation (4.33), the relationship of drawbar pull and the track slip can be predicted.

4.8 THE COEFFICIENT OF TRACTION AND TRACTIVE EFFICIENCY

The coefficient of traction C_{ct} is the ratio of tractive effort to the vertical load of the track and expressed by:

$$C_{ct} = \frac{F_t}{W} \tag{4.34}$$

The tractive efficiency η is the ratio of the output to input power of the track and expressed as:

$$\eta = \frac{P_{out}}{P_{in}} = \frac{F_h V}{2T\omega} \tag{4.35}$$

where

η = tractive efficiency.

P_{in} = input power, (kW).

P_{out} = output power, (kW).

F_h = total drawbar pull, (N)

V = travel velocity, (m/s)

T = input torque for one side shaft, (Nm).

4.9 MODELLING PROCEDURE

For both the flexible track and the rigid track models, the static vehicle weight was accepted to be supported only by the wheels. The sinkage of the front wheels were calculated based on Bekker's (1956, 1960) sinkage equation for solid wheels (equations 4.19 and 4.20). The sinkage of the rear wheels were accepted to be equal to that of the front wheels until the load increase caused by weight transfer, which lead to additional rear wheel sinkage.

The contact pressure at any point on the interacting surface was calculated based on the pressure sinkage relationship proposed by Bekker with equation (2.1) after which the sinkage at each point on the contact surface was determined by initial assumptions and the configuration of the track-terrain contact profile as described in the previous sections of this chapter. The tilt angle β was also taken into account for the contact pressure caused by sinkage.

The accumulated displacement j was calculated by equation (4.7) or equations (4.26) to (4.28). Equation (4.7) (p 4-9) was validated for the idealized contact pressure distribution. Equations (4.26) (p 4-17), (4.27) (p 4-17) and (4.28) (p 4-18) were applicable for the segments ABC, CDEF and FGH (Figure 4.4, p 4-13) respectively for the flexible track model. The tangential stress was then calculated from equation (4.2) (p 4-4), as described in the previous sections of this chapter. The total thrust for a specific level of slip was calculated by applying equation (4.11) (p 4-10) for the idealized uniform distribution or (4.23) (p 4-16) for the flexible track model. The parameters related to rubber-soil friction characterization were obtained from bevameter tests.

When the motion resistance was calculated by any of the equations (4.12) (p 4-10) for the uniform pressure distribution model, or equations (4.30) (p 4-18) and (4.31) (p 4-19) for the flexible track model respectively, the drawbar pull was the difference between the total tractive thrust and the calculated motion resistance.

The tractive thrust as well as the motion resistance could be calculated by either computer programming or spreadsheet coding. To utilize its advantage of simplicity, the spreadsheet method was mainly used for the calculations for this research.

The final results from the calculations were expressed as the relationship of either the tractive force or the drawbar pull versus the slip as was predicted.